X-641-68-207
PREPRINT

FEASIBILITY STUDY OF AUGER AND PHOTOELECTRON SPECTROSCOPY AS AN ANALYTICAL TECHNIQUE

L. I YIN
I. ADLER
R. LAMOTHE

JUNE 1968

GSFC
GODDARD SPACE FLIGHT CENTER
GREENBELT, MARYLAND

X-641-68-207

FEASIBILITY STUDY OF AUGER AND PHOTOELECTRON SPECTROSCOPY AS AN ANALYTICAL TECHNIQUE

L. I Yin
I. Adler
R. Lamothe

June 1968

GODDARD SPACE FLIGHT CENTER
Greenbelt, Maryland

CONTENTS

ILLUSTRATIONS

ILLUSTRATIONS (Continued)

ILLUSTRATIONS (Continued)

TABLES

FEASIBILITY STUDY OF AUGER AND PHOTOELECTRON SPECTROSCOPY AS AN ANALYTICAL TECHNIQUE

INTRODUCTION

I. General Background

Whenever a vacancy is created in one of the inner electronic shells of an atom a transition may occur in which the vacancy is filled by an electron from an outer shell. The excess energy, i.e. the difference between the binding energies of the two shells involved is often carried off by an emitted photon. Thus if the primary vacancy in the K shell with binding energy E_K is filled with an electron from the L_{II} shell with binding energy $E_{L_{II}}$ the emitted photon will have an energy $h\nu$ given by:

$$h\nu = E_K - E_{L_{II}}.$$

This for example is the well known $K\alpha_2$ characteristic x ray line. Alternatively this excess energy can be expended in the ejection of another electron from an outer shell of the same atom. This ejected electron is commonly known as an Auger electron named after its discoverer P. Auger.[1] Continuing with the previous example, if the Auger electron is ejected from the L_{III} shell the transition is denoted as KL_2L_3 with energy $E_{KL_2L_3}$ given by:

$$E_{KL_2L_3} = E_K - E_{L_{II}} - E'_{L_{III}}$$

where $E'_{L_{III}}$ in this case is the L_{III} shell binding energy when the atom is already ionized in the L_{II} shell. An approximation of $E'_{L_{III}}$ can be obtained by linear interpolation between the $E_{L_{III}}$ of the atom in question and that of the atom one atomic unit higher.

The relative intensities of these two alternate deexcitation processes is expressed in terms of the fluorescence yield. When the primary ionization occurs in the K shell the K fluorescence yield ω_K is

$$\omega_K = \frac{P_{KX}}{P_{KA} + P_{KX}}$$

where P_{KX} is the probability for K x-ray emission and P_{KA} the probability for K Auger emission. According to the estimates of Wenzel[2], P_{KA} is essentially independent of Z, the atomic charge whereas P_{KX} is proportional to Z^4 due to the

predominantly dipole character of K x rays. Therefore ω_K can be written in the form:

$$\omega_K = \frac{Z^4}{a_K + Z^4}$$

where a_K is a constant obtainable from experimental data. By taking into account screening and relativistic effects Burhop[3] modified the semiempirical formula to read:

$$\left(\frac{\omega_K}{1 - \omega_K}\right)^{1/4} = A + BZ + CZ^3$$

or

$$\omega_K = \frac{(A + BZ + CZ^3)^4}{1 + (A + BZ + CZ^3)^4}$$

where the constant A includes the effect of screening and C that of relativity. Using a least square fit to all known ω_K data Hagedoorn and Wapstra[4] obtained the following values for these constants:

$$A = -0.064, \quad B = +0.034, \quad C = -1.03 \times 10^{-6} .$$

With these values the error for ω_K is about 0.006 from Z = 10 to 92. The formula above shows that as Z decreases the fluorescence yield decreases sharply, with a corresponding relative increase in the Auger yield. As an example, the K fluorescence yield is only 0.013 for Mg (Z = 12). Therefore, when vacancies exist in the K shell of Mg, 99% of the deexcitation processes are via Auger electron emission.

II. Brief Review of Auger and Photoelectron Research

The characteristic monoenergetic x rays resulting from atomic deexcitations have been exploited in depth in many fields. In contrast, Auger and photoelectron spectroscopy has remained virtually unexplored until rather recently.

The major difficulty encountered in low energy electron spectroscopy is instrumental. High transmission, high resolution β-spectrometers for low energy electrons were not available until the invention of the iron-free double-focusing spectrometer of Siegbahn[5,6] . Recent (1962) instruments of this type are able to achieve momentum resolutions of about 10^{-4} .

Perhaps the largest contribution as a result of such high resolution, low energy β-spectrometers is the direct determination and revision of numerous atomic binding energies by the photoelectron method[7]. Characteristic x rays (usually $K\alpha$ radiations) whose energies are accurately known from x-ray spectroscopic data are used to eject photoelectrons from inner shells of atoms, and the kinetic energy of the ejected photoelectrons are measured with the β-spectrometer. The binding energy is then obtained directly as the difference between the x-ray photon and the ejected electron. The accuracy and simplicity of this method makes it far superior to the x-ray absorption edge method, and the energy of the photoelectron can be determined to within a fraction of an electron volt. Another consequence of the vacancy created by the x-ray photon is the emission of Auger electrons. In fact a large portion of Auger spectroscopy performed to date has utilized x-ray excitation and the iron-free double-focusing β-spectrometer.

There has been a most fruitful exchange between theorists and experimentalists on the Auger phenomenon in recent years. Prior to 1958 the theoretical treatment of Auger effect was expressed either in terms of pure j-j coupling or, in the light elements, pure L-S coupling. In 1958 Asaad and Burhop[8] calculated the Auger transition probabilities in terms of an intermediate coupling between the two inner vacancies of the final state of the atom for five values of Z from 25 to 80. Consequently the 6-line KLL spectrum of j-j coupling was modified into a 9-line spectrum. Using empirical values of E_K and E_L the positions of the lines as well as their relative intensities were also calculated in the intermediate coupling scheme. Experimentally, although Auger spectra of more than six lines had been reported[9, 10] the full 9-line spectrum was not observed until 1962 by Hörnfeldt et al.[11] in Sr, Zr and Mo. The observed energies of the Auger lines differed by as much as 50 to 75 eV from those predicted by Asaad and Burhop although the relative energy separation was in good agreement. A new set of constants based on these experimental results was then introduced into the semi-empirical expressions of Asaad and Burhop which was able to bring about good agreement between experiment and theory even for rather heavy elements. These adjusted parameters were used to calculate and tabulate Auger lines for $20 \leqslant Z \leqslant 100$.[12] Asaad[13] pointed out later that extreme j-j coupling is not fully approached even at $Z = 80$, and that intermediate coupling should still be applied in the relativistic calculations of KLL Auger spectrum of heavy elements.

Very little data were available on the KLL Auger spectra of light elements with $Z < 35$ before 1965. In the low-Z region both intermediate coupling and pure L-S coupling theories give the same results.[13] However large discrepancies of about an order of magnitude were found between the existing data and theory[14, 15] concerning the ratios of the total transition rates to the three different configurations: $(2s)^0(2p)^6$, $(2s)^1(2p)^5$ and $(2s)^2(2p)^4$. To remove such discrepancies

Asaad[16] introduced configuration interaction between the two configurations $(2s)^0$ $(2p)^6$ and $(2s)^2$ $(2p)^4$ for the J = 0 state in his calculations for low-Z elements. While subsequent experiments by Körber and Mehlhorn[17] on Ne (Z = 10), Fahlman et al.[18] on Na (Z = 11) and Mg (Z = 12), and Lui and Albridge[19] on Mn (Z = 25) showed good agreement with configuration-interaction calculations[16, 20] in general, the theory did not give correct relative individual line intensities. Very recently Johnston et al.[21] showed that no existing theoretical calculations is able to fit smoothly the available experimental data over a wide range of Z values.

From this brief review one can see that Auger spectroscopy today is still a very active field with unsolved problems both theoretically and experimentally.

III. Potential for Auger and Photoelectron Spectroscopy as an Analytical Tool

Aside from interest in the basic understanding of the Auger phenomenon and its use in the measurement of atomic binding energies which are of fundamental importance in atomic and nuclear physics, low energy electron spectroscopy is also potentially useful as an analytical tool. Several such possibilities will be mentioned.

Valence Effects—Making use of the high resolution available in the iron-free double-focusing β-spectrometer, binding energy shifts due to the chemical state of the atom have been observed in chemical compounds via photoelectrons[22-24] as well as Auger electrons[25]. Because of its directness and simplicity practically all elements can be studied by this method. In geochemistry where the valence state of iron is of crucial importance, its determination through electron spectroscopy may prove to be especially fruitful.

Chemical Analysis—The characteristic energies of the photoelectrons and Auger electrons suggest the possibility of chemical analysis. This idea has indeed been examined by a group of investigators in Upsalla[26]. From measurements of the intensities of photoelectron lines produced by some low atomic number elements they obtained precise chemical composition of the sample.

At comparable energies the penetrating power of charged particles is much less than that of photons. Therefore, under charged particle excitation such as electrons, protons and α particles the Auger electrons are generated near the top surface of the sample. In this fashion Auger spectroscopy is especially amenable to the study of surface-related phenomena. A recent article by Harris[27] lists a number of such possibilities using electron excitation. Some of these are summarized below.

Observation of Thin Layers—It has been observed in a low energy electron diffraction (LEED) apparatus that most of the Auger electrons of Au deposited on

Cu originate in the first two or four atomic layers. As little as 1/50 of a monolayer of Cs has been detected on a Si substrate and the intensity of the Auger line of K has been shown to be proportional to the fraction of monolayer coverage on a Ge substrate.

Qualitative Studies—Because of the enormous sensitivity to surface composition, Auger spectroscopy can be used in metallurgy to measure diffusion processes of elements to the free surface.

Adsorption Processes—By examining adsorption and desorption of gases on clean surfaces a potential exists for the study of oxidation and corrosion processes.

Transfer Processes—The observation of the transfer of materials by friction or evaporation through Auger spectroscopy needs to be examined as a complimentary method to tracer techniques.

Another application which occurred to the authors maybe of more fundamental interest. The paucity of data on the fluorescence yield of light elements points toward a need for measurements on its compliment, the Auger yield. One possible way to achieve this, or at least to establish the relative Auger yield among elements, would be to measure photoelectron and Auger electron coincidences. Here one uses the presence of photoelectrons with a given energy to signify the creation of vacancies in a particular shell, and the ratio of coincidence counts to photoelectron counts, after proper corrections, should in principle give the Auger yield. Analogously, photoelectron and fluroescence x ray coincidence measurement should give the fluorescence yield. This method avoids any theoretical estimate on the number of primary vacancies from photoelectric cross sections. In the case of higher shells, the energy of the photoelectron denotes precisely the subshell from which it is ejected; therefore no estimate is necessary about the vacancy distribution among subshells. By definition, the coincidence method requires two electron spectrometers. However, since high resolution is no longer necessary, coarser instruments of the type described in the following sections will be adequate. Should the coincidence method prove feasible it can be used to study other phenomena related to multiple-ionization such as Coster-Krönig transitions and x-ray satellites (x ray-electron coincidence).

The review in Section II showed that most of the electron spectrometers today are of the high resolution magnetic type, although Melhorn[28, 29] , in the study of Auger electrons from gaseous samples, did employ an electrostatic analyzer of cylindrical geometry. Due to the high precision requirements these instruments are physically large, difficult to construct and require careful magnetic shielding. Data collection time is also very long. For some applications mentioned above, coarser and smaller spectrometers with degraded resolution may suffice or

even be preferable. This document will describe such an instrument and some of the preliminary results obtained with it.

INSTRUMENTATION

I. Spectrometer

Although the spherical condenser or "Keplertron" type of β-spectrometer has been designed, analyzed and constructed[30-36] in the past, it has never become popular in nuclear physics mainly because of its practical limitation in analyzing electrons with energy higher than about 100 keV. Recently, however, there has been renewed interest in such spectrometers for the measurement of low energy charged particles in space experiments[37-39]. The weight and power requirements in addition to the introduction of magnetic fields into the spacecraft make the magnetic analyzers undesirable in such experiments.

The original design of the spherical spectrometer described here is due to Henke[40]. It consists of two concentric metallic hemispheres of inner and outer radii 2.5" and 3.0", and entrance and exit slits of dimension 0.045" x 0.730" diametrically located on a 2.75" radius circle as shown in Figure 1. The hemispheres are electrically insulated from each other by sapphire balls and the slits are insulated from the hemispheres by 0.010" thick mylar sheets as well as Fluorosint T-3 (ceramic fluorocarbon) material.

When a voltage V is applied between the hemispheres as shown, an electron entering the spectrometer is subjected to the central inverse-square electrostatic field established by the hemispheres. From conservation of angular momentum and total energy, its motion is in a plane and its orbit elliptic. A consequence of the inverse-square field is that electrons with the same energy have the same major axis $2r_o$ in their elliptical orbits where r_o is the radius of the "central" circular orbit[41]. The condition for circular orbit gives

$$\frac{K}{r^2} = \frac{mv^2}{r} = \frac{2eE}{r}$$

where $$K = eV\frac{R_o R_i}{R_o - R_i}$$ is a constant,

and $V = V_i - V_o$ is the voltage difference between the hemispheres. The other symbols are: r, the radial coordinate of the electron; e, its charge; E its energy; m, its mass and v, its velocity. R_o and R_i are respectively the radius of the outer and inner hemisphere, and V_o and V_i their respective voltages. It follows that for

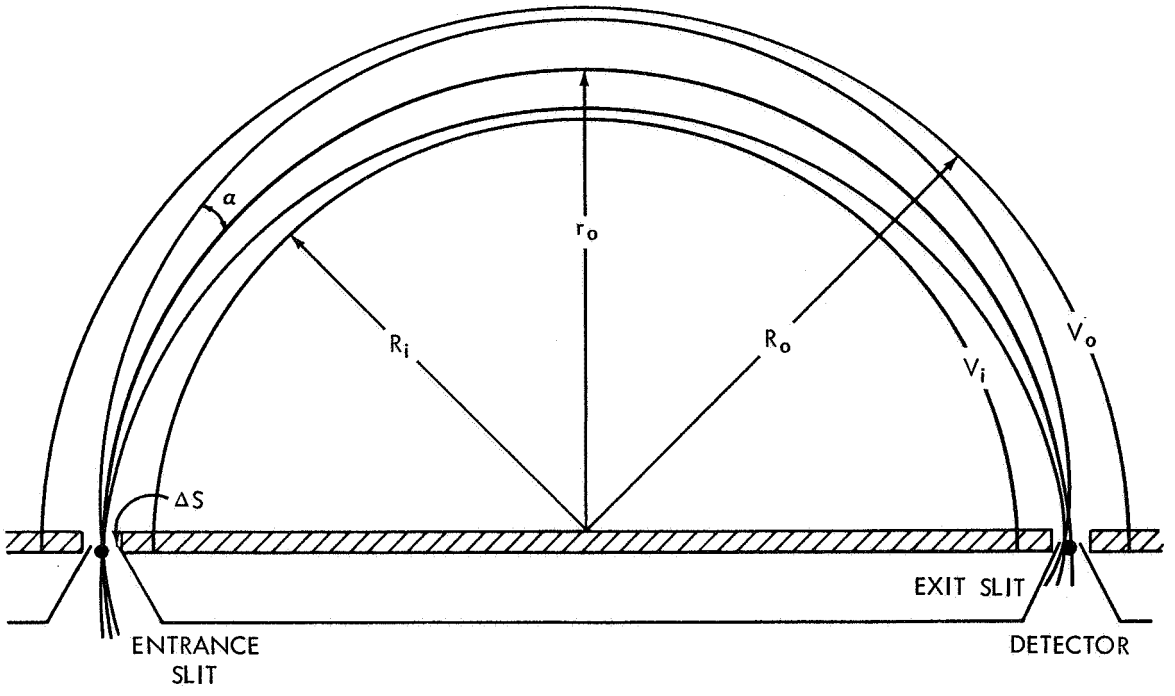

$$R_i = 2.5"$$

$$R_o = 3.0"$$

$$r_o = \frac{R_i + R_o}{2} = 2.75"$$

$$\Delta S = 0.045"$$

$$V_o = 0$$

$$V = V_i - V_o = V_i$$

$$eV_{slit} = \frac{K}{r_o} - \frac{K}{R_o} = eV_i \frac{R_i}{R_o + R_i} = \frac{5}{11} eV_i$$

$$K = eV \frac{R_o R_i}{R_o - R_i}$$

$$V = E \left[\frac{R_o}{R_i} - \frac{R_i}{R_o} \right] = \frac{11}{30} E$$

Figure 1. Sketch of the Hemispherical Spectrometer and its Operating Parameters.

$$r = r_o = \frac{R_o + R_i}{2} ,$$

$$V = E\left(\frac{R_o}{R_i} - \frac{R_i}{R_o}\right)$$

In the case of the spectrometer described here, where $V_o = 0$, $V = V_i$,

then $$E = \frac{30}{11} V_i .$$

This is the kinetic energy of the electrons for which the spectrometer voltage V is set. It is easily seen that because of spherical symmetry such a hemispherical spectrometer is naturally double-focusing when entrance and exit are diametrically situated.

If Δs is the entrance and exit slit width and a the incident angle as shown in Figure 1, by assuming $\Delta s/2r_o \ll 1$, $a \ll 1$, Henke[40] showed that the percentage resolution of the spectrometer is

$$\frac{\Delta E}{E} \simeq a_m^2 = \frac{\Delta s}{2r_o} ,$$

where a_m, the maximum value of $|a|$, is shown to be $(R_o - R_i)/2r_o$. It is seen that the percentage energy resolution is only a function of spectrometer geometry and is constant for a given spectrometer. In comparing the luminosity-resolution equation with five other types of magnetic β-spectrometers he showed that in the range of $0.1\% \leqslant \Delta E/E \leqslant 20\%$ the hemispherical spectrometer has the greatest luminosity.

II. Detector

The electron detector used in conjunction with the spectrometer is a curved channel electron multiplier with a slot on its side comparable in shape and size to the exit slit of the spectrometer. A sketch of the multiplier is shown in Figure 2. This type of electron multiplier is made from a hollow glass tubing whose inner surface is coated with a semiconducting material favorable for secondary electron emission. When a dc potential is applied to its ends as shown in Figure 2, secondary electrons which are generated by the input electrons are accelerated towards the output. However, due to the transverse component of their velocities as they are liberated from the channel surface, these

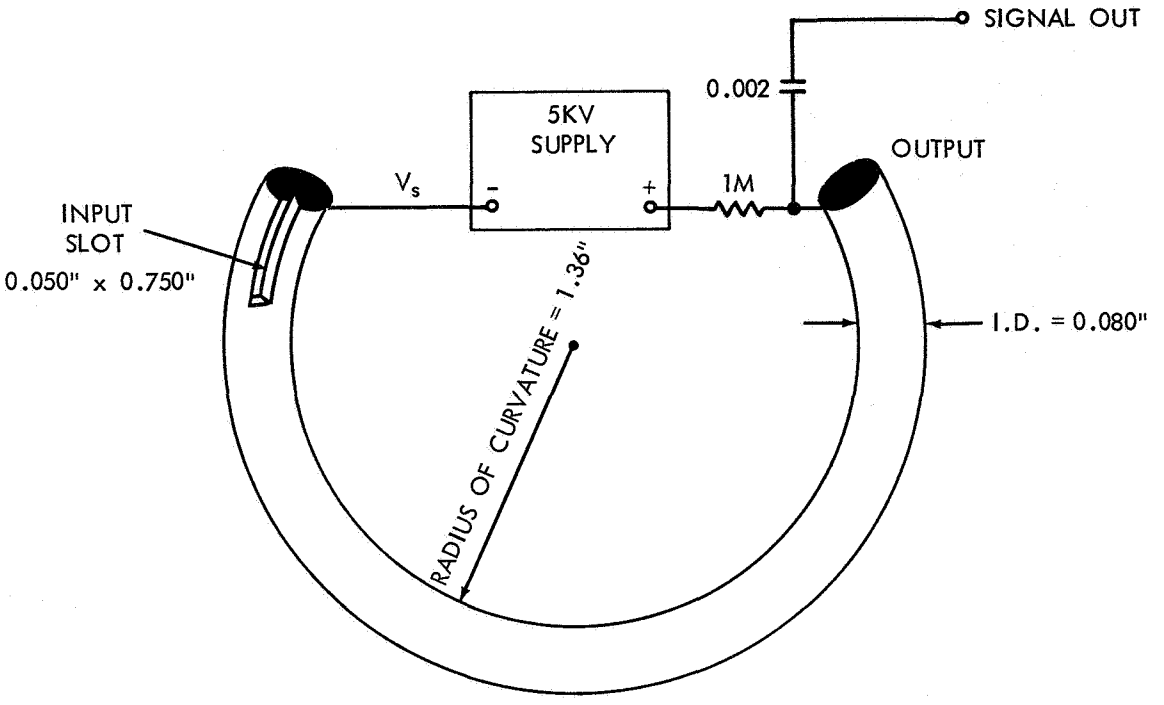

Figure 2. Channel Electron Multiplier Used with the Hemispherical Spectrometer.

electrons inevitably collide with the channel wall before they are able to travel any appreciable distance. At sufficiently high applied potentials the secondary emission ratio on the average is greater than unity per collision, and thus a multiplication process is initiated. In the case of the specific multiplier used here the average gain is 1.6×10^8 at 3.3 kV in the pulse counting mode.

The electrons from the spectrometer are detected as charge pulses (digital) rather than currents (analog) from the channel multiplier output. Besides the many orders of increase in sensitivity, the digital mode is superior in that it is also independent of gain shift in the multiplier. This is because in the analog mode the output current is linear with input current only if the gain of the multiplier is a constant. Should the gain become intensity-dependent, or change for any reason, the linear relationship no longer holds. In the digital mode, as long as the output pulse height is larger than the instrumental noise level, each event is registered by the scaler regardless of pulse height fluctuations. In this respect the channel multiplier has an important additional advantage over most electron multipliers. This lies in the capability of the channel multiplier to produce not only large pulse heights but also peaked pulse height distributions due to space-charge limitation[42]. In other words, at sufficiently high voltages all the output pulses from single electron inputs have nearly uniform amplitude. Figure 3a shows the pulse height distribution of the channel multiplier used in this spectrometer with monoenergetic input electrons. The peak of the

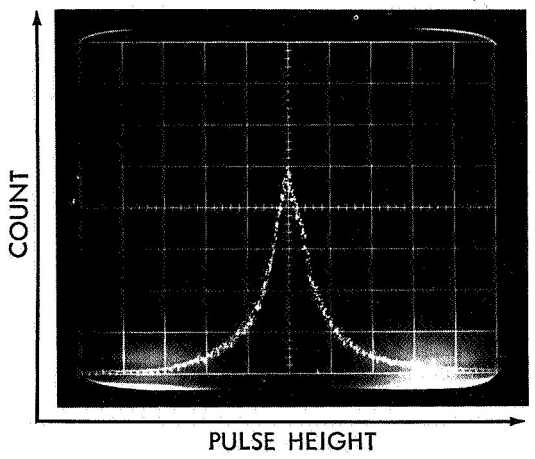

Figure 3a. Pulse Height (gain) Distribution of the Channel Multiplier for Single Electron inputs. Operating Voltage: 3300V. Gain at Peak of Distribution: 1.6×10^8 Input Intensity: 600 C/SEC.

distribution corresponds to a gain of 1.6×10^8. The channel voltage was 3.3 kV and the counting rate was 600 c/sec. In contrast, for most multipliers the pulse height distribution for single electron inputs is very broad and almost exponential in shape, with the preponderance of pulses in the very low amplitude region as sketched in Figure 3b. It is therefore inevitable that a portion of signals will have amplitudes comparable or smaller than the instrumental noise level and consequently discarded with the noise. The peaked pulse height distribution of the channel multiplier allows all input electrons which are able to produce secondary electrons to be counted. Furthermore, since instrumental noise can easily be reduced to two orders of magnitude below the signal level, should the channel suffer a gain loss either permanently or dynamically, such as at extremely high counting rates, no signal loss will result. It is for these reasons that a channel multiplier was chosen to be the detector in the hemispherical spectrometer.

III. Electronics

The block diagram of the spectrometer and its associated electronics is shown in Figure 4. Most of the electronics are standard pulse circuitry. The multichannel analyzer is used in the multiscaler mode to display the differential energy spectrum. The dwell time at each channel can be varied up to 10 sec by the time-base generator. The ramp generator, designed and constructed by WTA Co., supplies a voltage ramp to the inner hemisphere as well as the slits. It has a full range of 3000 V. The ramp slope can be varied continuously from 6 V/channel to 0.1 V/channel which correspond to electron energy increments of 16 eV/channel to 0.27 eV/channel. The starting voltage of the ramp can be set anywhere from 0 to 3000 V by the separate dc bias supply. The measured linearity of the ramp is

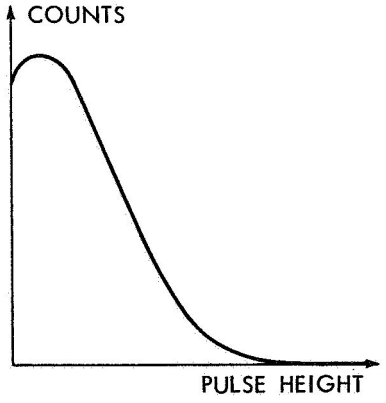

Figure 3b. Pulse Height Distribution of Most Electron Multipliers for Single Electron Inputs.

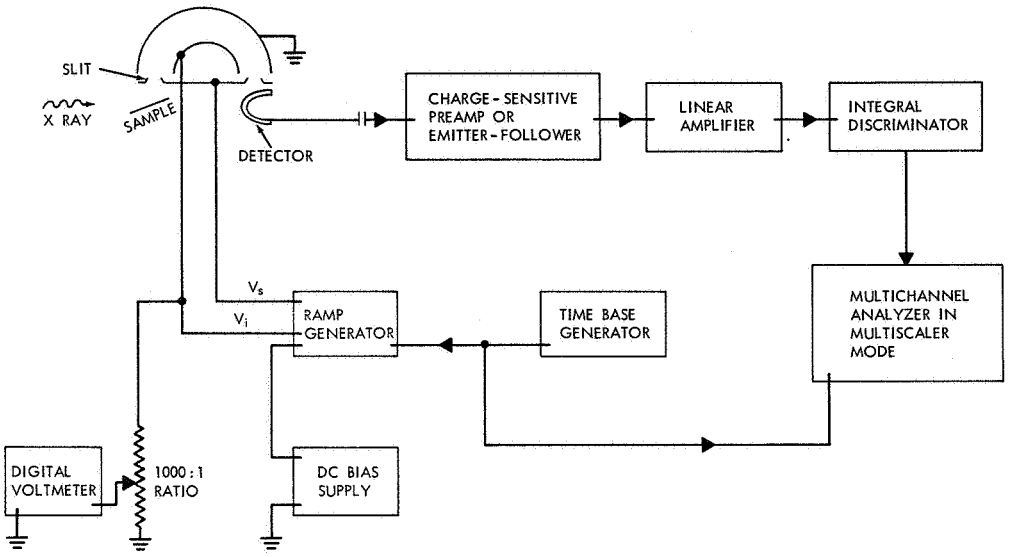

Figure 4. Block Diagram of Spectrometer and Associated Electronics.

better than 1%. This arrangement allows maximum flexibility in data accumulation and display. The response time of the setup is only limited by the pulse-pair resolution of the scaler in the multichannel analyzer rather than any mechanical device such as an x-y recorder.

IV. The X-ray Tube

The demountable high power soft x-ray source is the design of Deslattes and Simson.[43] Minor modification has been made to pump the x-ray tube and the spectrometer side of the chamber simultaneously so that there is little pressure differential across the x-ray tube window. The window then serves only as an electron absorber and x-ray filter. A Yee and Deslattes[44] type of emission stabilizer is used to maintain the emission current of the x-ray tube at a given level during data accumulation to insure stable x-ray intensity, assuming no short-term changes occur in the x-ray energy spectrum. There is no facility for changing x-ray anodes without breaking the vacuum. However, anode changes can be made quite easily once the x-ray tube is at atmospheric pressure.

V. Vacuum System

A crude oil diffusion pump system is being used for the present feasibility studies. The operating pressure is usually in the 10^{-6} torr range. Contamination of the x-ray tube anode and the sample is therefore inevitable. Since the Auger and photoelectron spectra are extremely sensitive to surface conditions,

semi-quantitative and quantitative information can only be obtained in a "clean" high vacuum system. Such a system is now being designed.

TECHNIQUE OF ANALYSIS

I. Calibration of Spectrometer

There are two factors that concern us in the measurements of the electron beam intensities. These are the detection efficiency of the Channel Multiplier, defined as the ratio of the number of electrons counted to those incident on the detector and the collection efficiency which is the ratio of the number of electrons entering the detector to those emerging from the spectrometer.

The detection efficiency depends on the secondary emission ratio of the channel surface which in turn depends on the energy of the incoming electrons. Fortunately this secondary ratio varies very slowly for most materials in the range of 100 eV to 10 keV.

There are two methods for maintaining a nearly constant detection efficiency. One is to bias the detector entrance slit with respect to the spectrometer exit slit so that all electrons entering the detector will have the same energy. The second method which takes advantage of the constancy of the secondary emission ratio described above, keeps the detector and exit slits at the same potential, i.e., a field free region between the exit slit and the detector. Since we are working with a detector entrance slit comparable in dimensions to the exit slit of the spectrometer the second or field free method is the more effective. The use of the bias technique involves the application of either accelerating or decelerating voltages between the detector and exit slit depending on the electron energies. These voltages will affect the focus of the electrons arriving at the detector which in turn causes changes in collection efficiency. By contrast in the field free arrangement one can achieve an almost constant collection and detection efficiency.

The spectrometer characteristics were calibrated with monoenergetic electrons from an electron gun. The gun consists of a flat tungsten ribbon placed 1" above and across the entrance slit to simulate approximately an extended source in the radial direction. The energies of the electrons were established by a variable 0-3000 V dc supply having a calibration accuracy of 1%. No focusing other than that of the accelerating voltage was provided. At a given electron energy, the position of the peak was established by manually changing the hemisphere voltage. This eliminates any possible non-linearity introduced by the ramp generator. The results of such a calibration is shown in Figure 5. It is

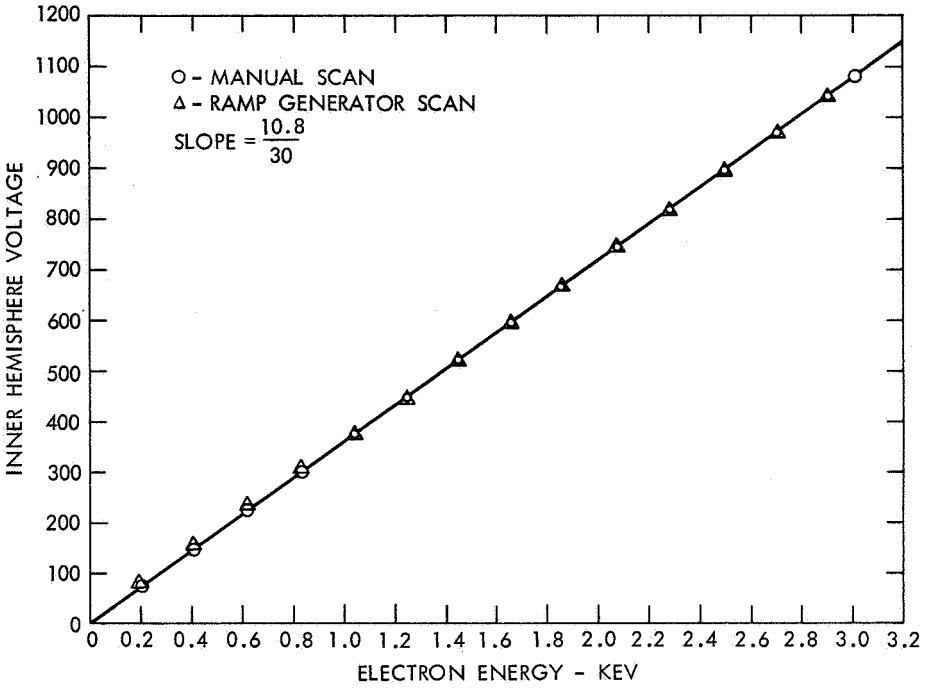

Figure 5. Energy Calibration of Spectrometer and Linearity of Ramp Generator.

seen that the linearity of the spectrometer is good to within the thickness of the pencil line. The measured slope is 10.8/30 as compared to the theoretical value of 11/30. This experimentally obtained calibration curve is used to analyze subsequent data.

The linearity of the ramp generator was then calibrated by scanning the ramp throughout the same energy range and the data printed out from the multichannel analyzer. Knowing the total hemisphere voltage range and the number of channels used in the multichannel analyzer, the peak positions were calculated and compared with the data obtained manually. As shown in Figure 5 the linearity of the ramp generator is off by approximately 1% in the low energy end.

The energy resolution of the spectrometer-plus-detector system was measured by scanning through a single monoenergetic peak in very small increments with the ramp generator. The peak position and full width at half maximum were then calculated from the print-out data. One such peak at 2075 eV is shown in Figure 6. The measured resolution $\Delta E/E$ is 0.61%. In fact, at six typical energies between 400 and 3000 eV the average measured percentage resolution was found to be $(0.60 \pm 0.07)\%$ and independent of energy to within experimental error. The side peaks in Figure 6 are probably due to scattering inside the hemispheres[34, 39]. No effort has been made to eliminate them although methods do exist[34]. The measured resolution is slightly better than the

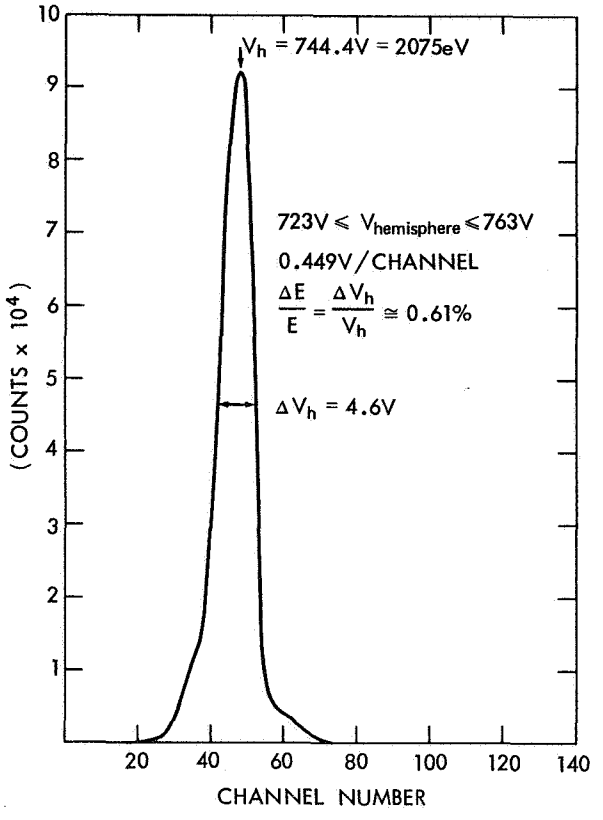

Figure 6. Resolution of Spectrometer at 2075 eV.

expected resolution of 0.8%. Other than experimental errors and theoretical approximations, one cause for the discrepancy maybe due to the fact that the entrance slot of the detector is comparable in size with the exit slit of the spectrometer. Since the distance between the two is about 0.75" (the closest mechanically possible distance) the slot serves as a collimator and thereby reduces the effective width of the exit slit and improves the resolution.

II. Electron Excitation

In the early stages of this feasibility study attempts were made to obtain Auger spectra with electron excitation. The vacuum system used at that time was a small ion pump without trapping. A simple electron gun similar to the one described in the previous section with the addition of a collimating hole was used as the electron source. During data taking the ion pump was turned off so that there was no background contribution from the ion pump. Admittedly, the system left much to be desired. A piece of Mg metal was used as a sample and was bombarded with 1440 eV electrons from the electron gun. The resulting

spectrum is shown in Figure 7. Figures 7a and 7b are logarithmic and linear displays of the same spectrum. The sharp 1440 eV elastic scattering peak is easily seen. Also discernible are the Auger peaks of Mg, Na, O and C. The presence of Na might be due to careless handling of the sample; and the C peak indicates the presence of organic contaminants. Due to overflow in the display the 1440 eV peak cannot be seen in 7b. However, the O peak is slightly clearer. Because of inadequate shielding of the detector some electrons do enter the detector without going through the spectrometer. These electrons contributed to the high background even above the excitation energy. It should be noted also that the energy scale in Figure 7 is rather non-linear due to the motor-driven ramp generator used at the time of the experiment. Later it was replaced by the electronic ramp generator described in Section II of INSTRUMENTATION.

Although the instrumentation was extremely crude during this phase of experimentation the inherently intense background caused by the scattered primary electrons make even qualitative intensity features of the Auger spectra difficult to discern. Therefore recent efforts have been concentrated on x-ray excitation where most of the background is expected to be generated by the sample itself. Moreover, both Auger and photoelectrons can be studied in x-ray excitation.

Recently, in two successive papers,[45, 46] Harris gave an excellent demonstration of the enormous sensitivity of Auger spectra toward various surface phenomena. In order to enhance the presence and positions of the electron-excited Auger peaks, his spectra were differentiated electronically. However, since peaks of various intensities with the same shape will appear to be identical after differentiation, intensity information can only be obtained from an undisturbed spectrum.

III. X-ray Spectra

As a matter of convenience most of the electron spectra were obtained with either Al Kα or Cr Kα excitation. The x-ray spectra from these anodes at various excitation voltages were observed nondispersively with a proportional counter and displayed on the multichannel analyzer. Optimum operating voltages were chosen where the x-ray spectrum for a given anode was essentially monoenergetic with little continuum background. This was to insure that the photoelectrons also remained monoenergetic. Figure 8 shows two typical x-ray spectra each accompanied by a Mn Kα (Fe^{55} source) spectrum for the purpose of energy calibration. In both cases the x-ray tube had a 0.001" thick Al window. A sealed proportional counter filled with 90% Ar and 10% methane gas at 1 atm pressure and a 0.005" Be window was used as the detector. The counting

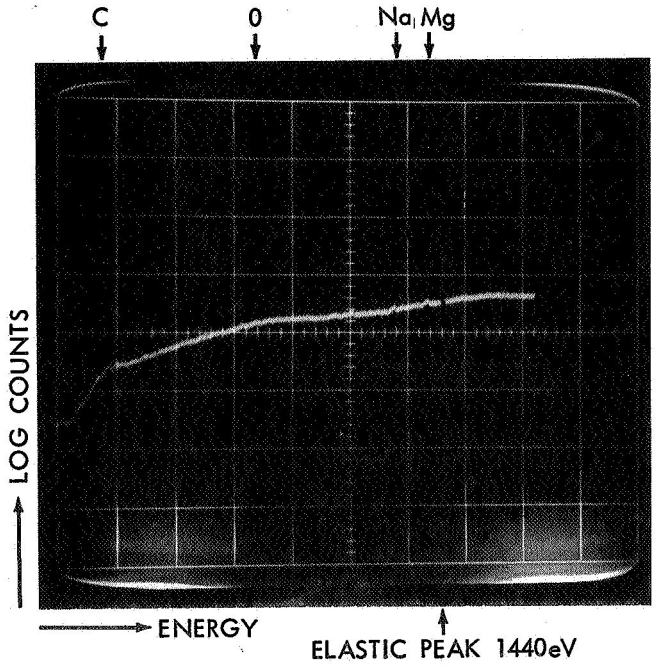

a. Semi-log display of Auger spectrum.

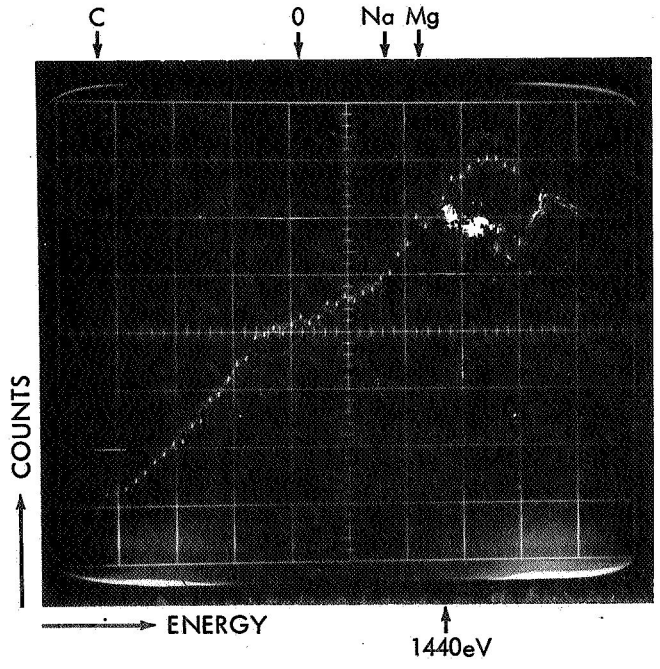

b. Linear display.

Figure 7. 1440 eV electron excitation of Mg sample.

rate for all spectra was kept approximately equal so as not to cause any gain shift in the proportional counter due to variations in the counting rate. Figure 8a is the Al anode spectrum at 5 kV excitation voltage and 8b the Mn Kα calibration. The peak at the very low energy side in both spectra was due to electronic noise. Figure 8c is the Cr anode spectrum at 15 kV excitation voltage and 8d its Mn Kα calibration.

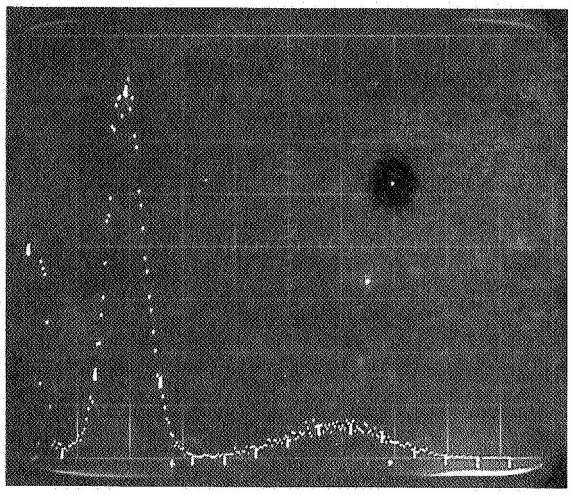

a. Al anode at 5 kV.

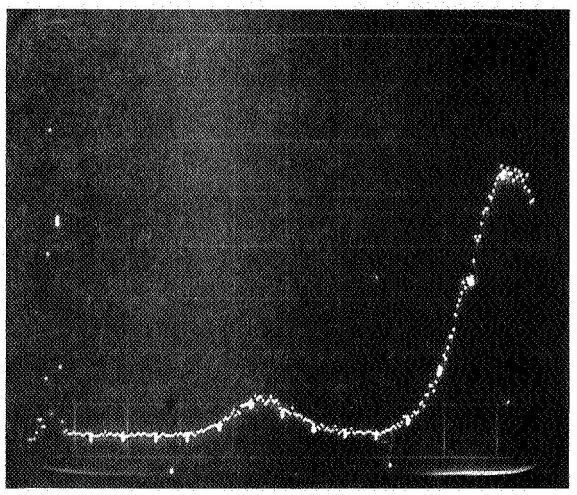

b. Mn Kα calibration for a.

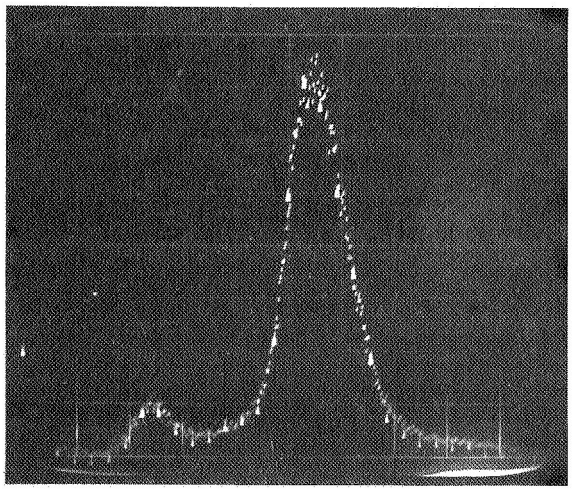

c. Cr anode at 15 kV.

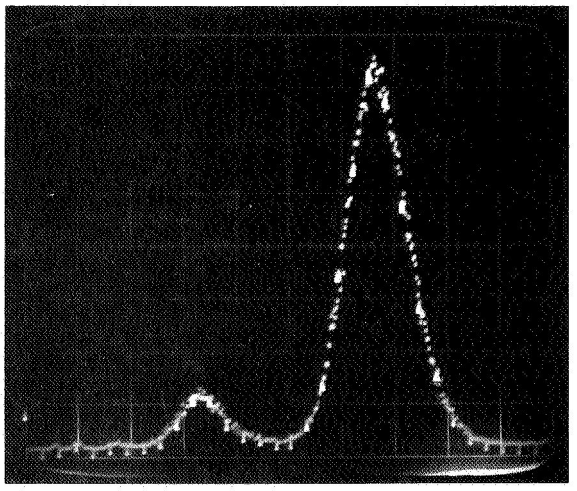

d. Mn Kα calibration for c.

Figure 8. X-ray spectra of Al and Cr anodes.

AUGER AND PHOTOELECTRON SPECTRA

I. Effect of Sample Potential on the Position of Peaks

In order to have accurate information on the true energy of the electrons ejected from a sample the sample must be at the potential of the entrance slit of the spectrometer. This requirement presents obvious difficulties in the case of insulating samples. An example of the shift in the peak positions as a result of sample potential is shown in Figure 9. A graphite disc was used as the sample; Al Kα xrays were the sources of excitation. The x-ray tube was operated at 5 kV with an anode current of 142 ma. The x-ray spectrum can be found in Figure 8a. In Figure 9a the graphite sample was electrically connected to the entrance slit so that they were at the same potential. The two clearly visible peaks are due to C Auger electrons at 268 eV and C photoelectrons at 1202 eV. From the range of voltage scan by the ramp generator, the total number of channels used in the analyzer and the calibration graph in Figure 5 the calculated positions of these peaks were 265 eV and 1195 eV respectively. The agreement with theoretical values was good. In Figure 9b the graphite sample was disconnected from the entrance slit electrically and left floating. The shift in positions is quite obvious. Since the sample is conductive the amount of shift in this case (about 220 eV for the photoelectron peak) is as if the sample was at ground potential. For an insulating sample such as a glass microscope slide the amount of shift is much less predictable.

In order to identify unknown peaks in an unknown sample it is therefore necessary to establish the potential of the sample to be as close to that of the entrance slit as possible. To this end the following methods were attempted.

A 0.0002" thick, 30 mesh Ni screen was placed over the microscope slide sample and connected electrically to the entrance slit. The peaks of the sample shifted sufficiently towards the theoretical values to become identifiable although the general shape of the spectrum was distorted because of the presence of the Ni screen. The same was true when the Ni screen was placed over a bricket made from powdered samples. This method however proved to be quite cumbersome. A more satisfactory method was found in the use of conductive substrates. Excellent results were obtained when a very thin layer of powdered sample mixed in either acetone or H_2O was brushed onto a graphite disc and the carrier subsequently evaporated off. When the disc was at the potential of the entrance slit the energy of the peaks could be accurately determined. An example using this method is shown in Figure 10. Al_2O_3 powder on a graphite disc was excited by Cr K x-rays with the x-ray tube operating at 16 kV and an anode current of 50 ma. Figure 10a shows the spectrum with the graphite floating and 10b, with

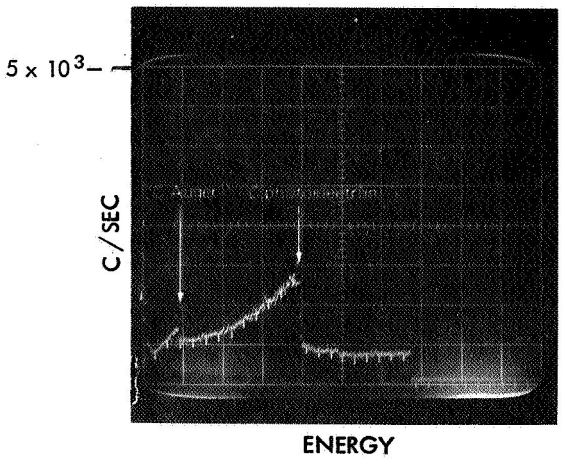

a. Sample at same potential as entrance slit.
C Auger: 268 eV, C photoelectron: 1202 eV

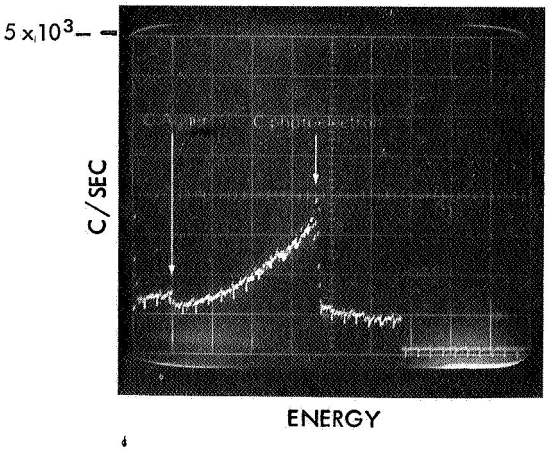

b. Sample floating.

Figure 9. Effect of sample potential on Auger and photoelectron spectrum.

the graphite at the slit potential. The peaks observed in 10b are sufficiently close to the theoretical value for unambiguous identification.

II. Effect of Incidence Angle and Sample Thickness

The majority of electrons generated in a solid sample suffer energy losses on their way out of the sample. Although these losses occur in small discrete increments via the excitation of atoms, molecules, valence electrons or collective plasma oscillation, the total energy loss of many electrons is large in

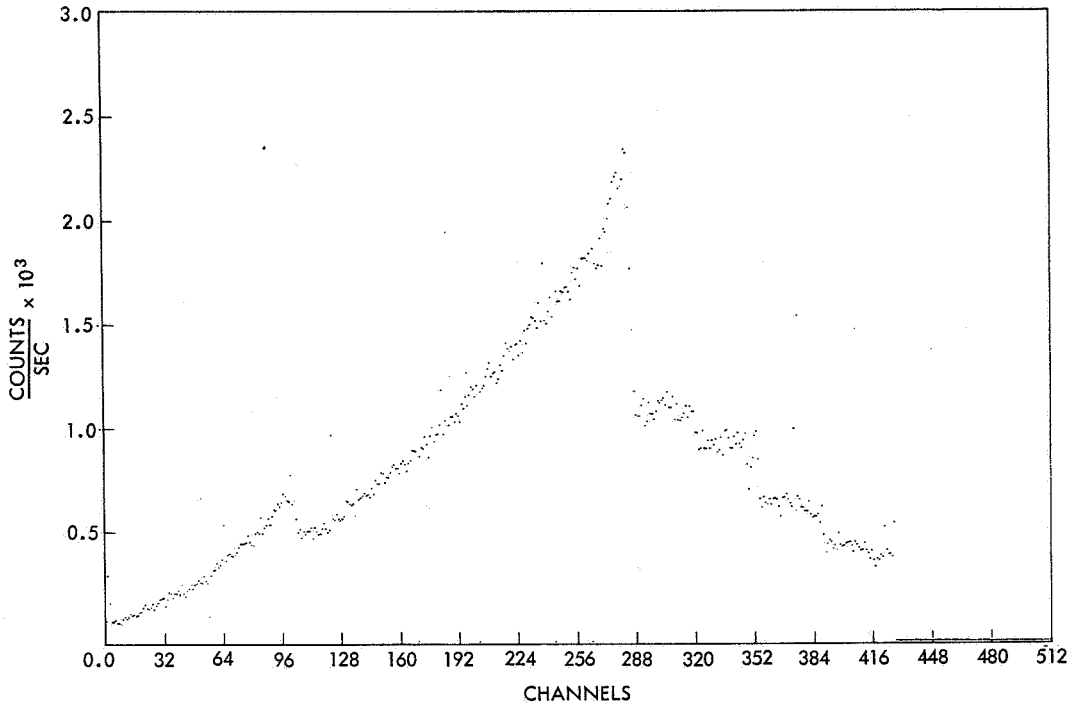

a. Graphite floating.

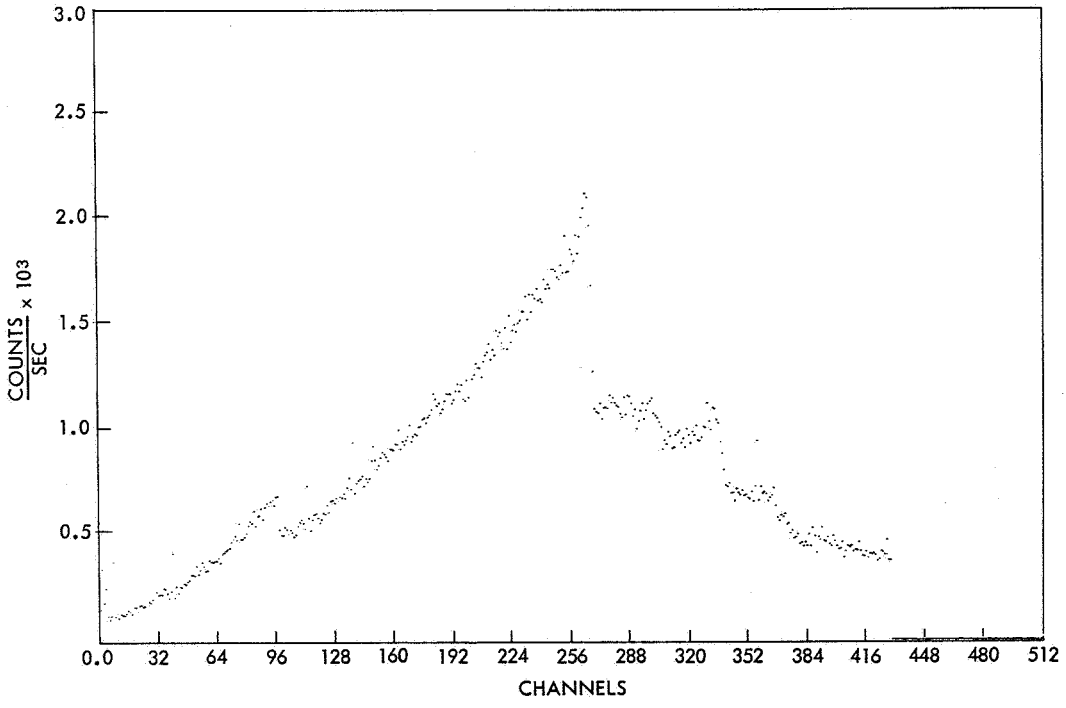

b. Graphite at entrance slit potential.

Figure 10. Effect of sample potential on Auger and photoelectron spectrum. Al_2O_3 powder on graphite disc, Cr Kα excitation. X-ray anode at 16 kV, current 50 ma.

a thick sample. This accounts for the continuum spectrum on the low energy side of each monoenergetic line in a given sample. It is therefore reasonable to expect that the shape of the spectra should be affected by the thickness of the sample as well as the incidence angle. This effect is demonstrated in Figure 11. Figure 11a shows the spectrum of Al_2O_3 powder on a graphite disc at an incidence angle of about 45°. Figure 11b is the same spectrum with the sample at near grazing from the incident x-rays. The sharpened features as well as the increased intensities in Figure 11b are obvious.

For a very thin sample one expects a still more sharply defined spectrum due to the increasing number of electrons which can emerge without energy loss. Furthermore, the shape of the spectrum should not be as sensitive to the angle of incidence as with the thick sample. This was indeed true when a 6-μ thick mylar with about 500 Å of evaporated Al was used as a sample. The spectrum is shown in Figure 12. The Al peaks are seen to be much sharper than those of Figure 11. This spectrum shape was also found not to change noticeably when the angle of incidence was varied or when the x-rays were incident from the back of the mylar so that the sample was excited by the transmitted x-rays. Both Figures 11 and 12 were obtained with Cr K x-rays.

III. Typical Spectra

It should be emphasized that the spectra exhibited here are preliminary results obtained in a rather crude fashion. The vacuum was usually around 10^{-6} torr and no effort was made to clean the sample surface of contaminants such as by heating or glow discharging. Although the resolution of the spectrometer has been determined, the collection efficiency of the entire system as a function of energy is yet unknown. Therefore no attempt was made to obtain quantitative information such as intensities of the lines or the relative abundance of elements. However the features of these spectra clearly indicate the inherent capability for quantitative analysis.

All the spectra were taken with a dwell time of 1 sec per channel. Figures 13-16 show the spectrum of a microscope slide using Al Kα x rays as excitation source. The identification of the peaks was accomplished with the method described in Section I. Figure 13 is the coarse scan of the entire energy range. The prominent features are the Auger electrons and photoelectrons of Na, O and Mg. Of course no K-shell photoelectrons or KLL Auger electrons can be excited from elements heavier than Mg. The presence of C was found in all spectra and indicated hydrocarbon surface contamination of the sample. Figures 14-16 show typical fine scan features of the same sample in three energy regions. Figure 14 is a scan of the very low energy region. Notable in this region is the

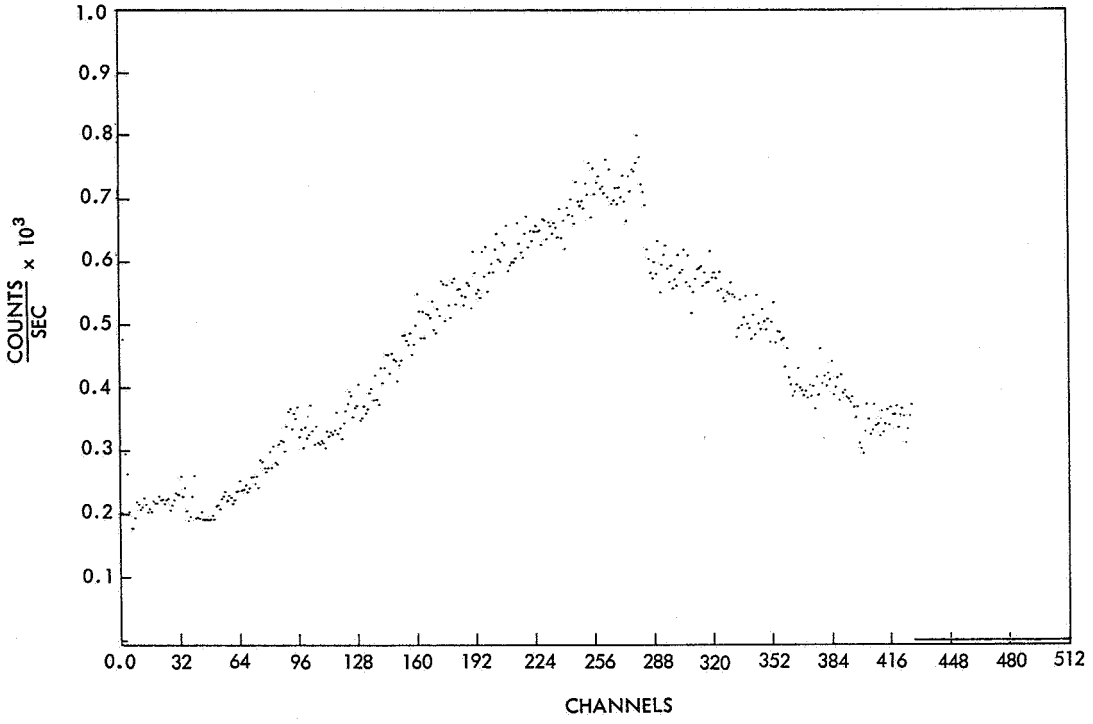

a. Incidence angle at about 45°, 1 x 10^3 c/sec full scale.

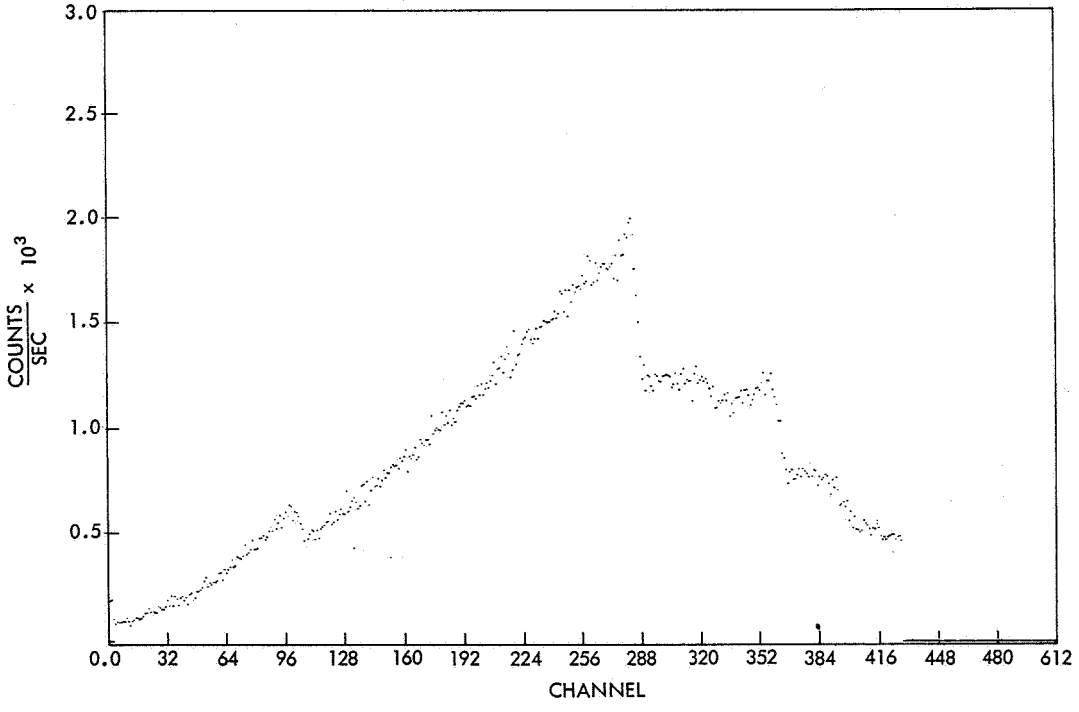

b. Incidence angle near grazing, 3 x 10^3 c/sec full scale.

Figure 11. Effect of incidence angle on Auger and photoelectron spectrum. Al_2O_3 powder on graphite disc, Cr Kα excitation. X-ray anode at 16 kV, current 50 ma.

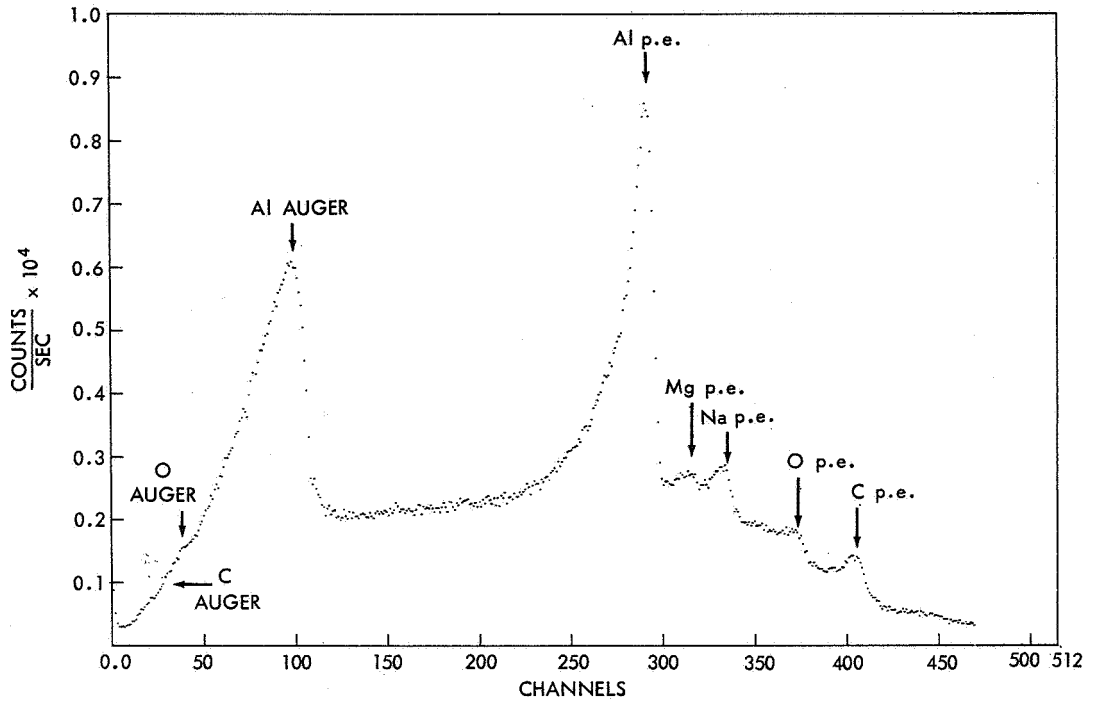

Figure 12. Effect of sample thickness on Auger and photoelectron spectrum. ~500 Å Al evaporated on 6-μ myler, Cr Kα excitation. X-ray anode at 15 kV, current 50 ma. 1 X 10^4 c/sec full scale.

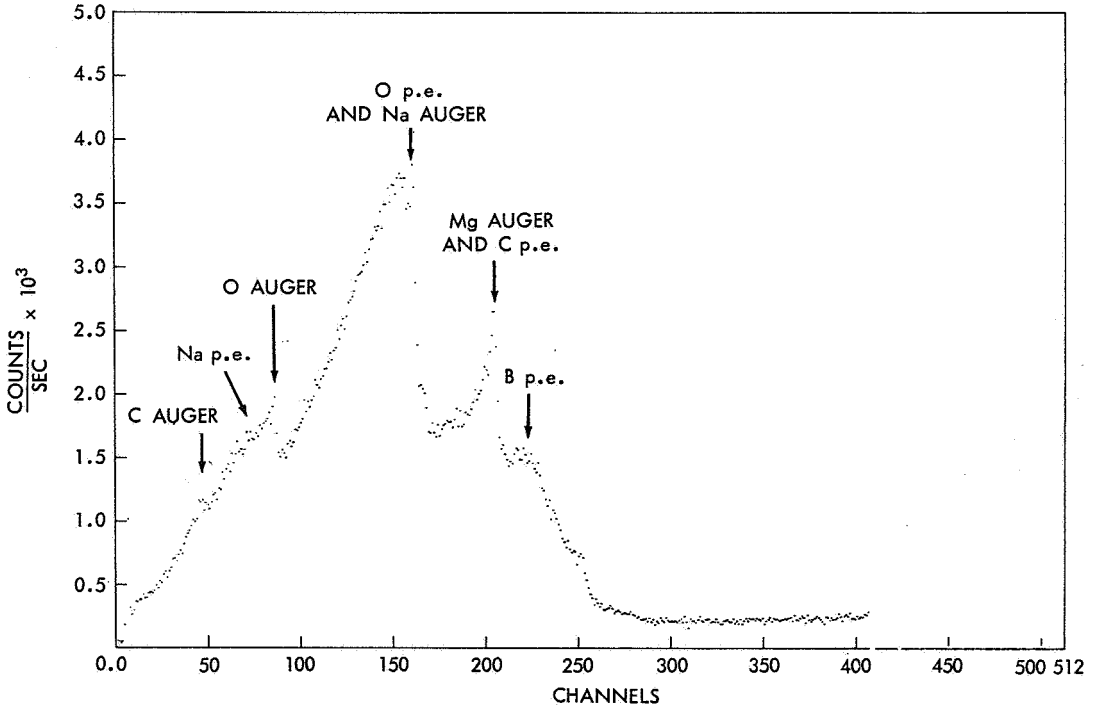

Figure 13. Auger and photoelectron spectrum of microscope slide, Al Kα excitation. Coarse scan 0-2400 eV.

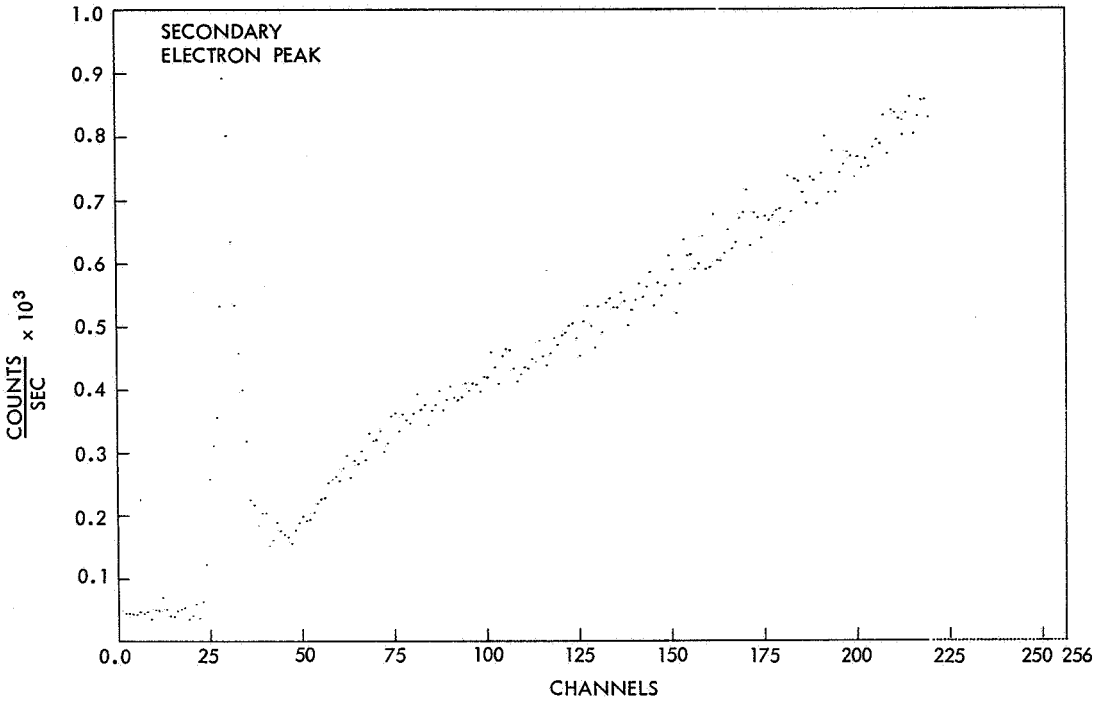

Figure 14. Fine scan of microscope slide sample. 0-250 eV, Al Kα excitation.

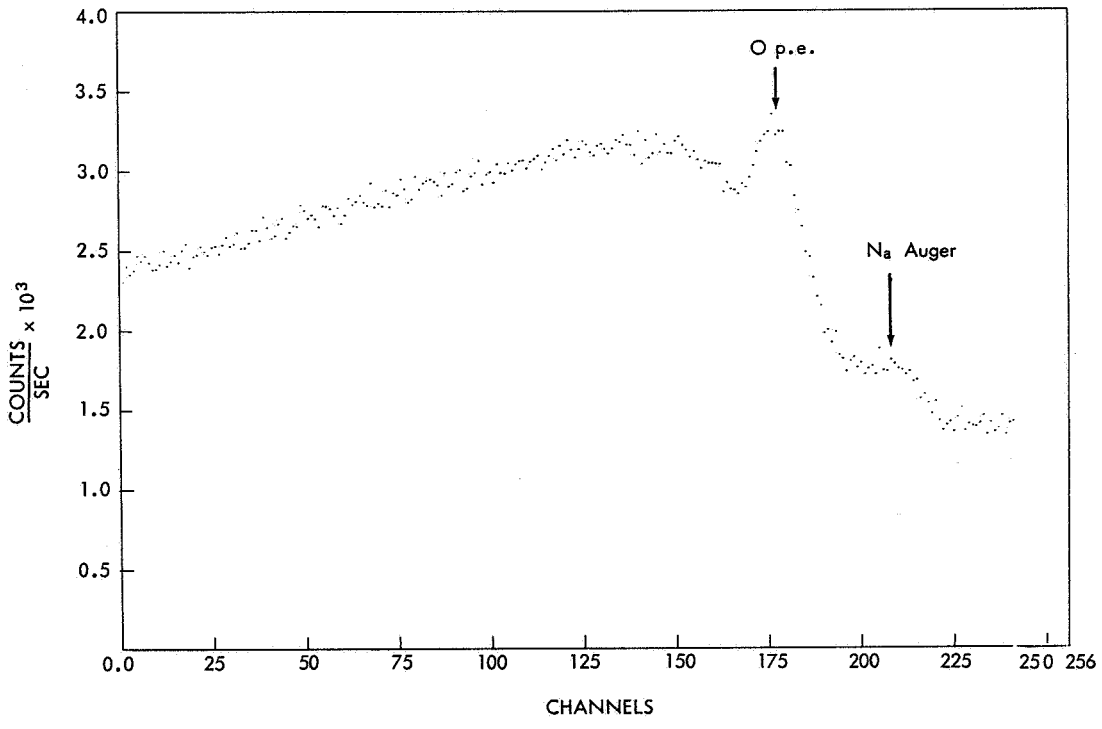

Figure 15. Fine scan of microscope slide sample. 790-1080 eV, Al Kα excitation.

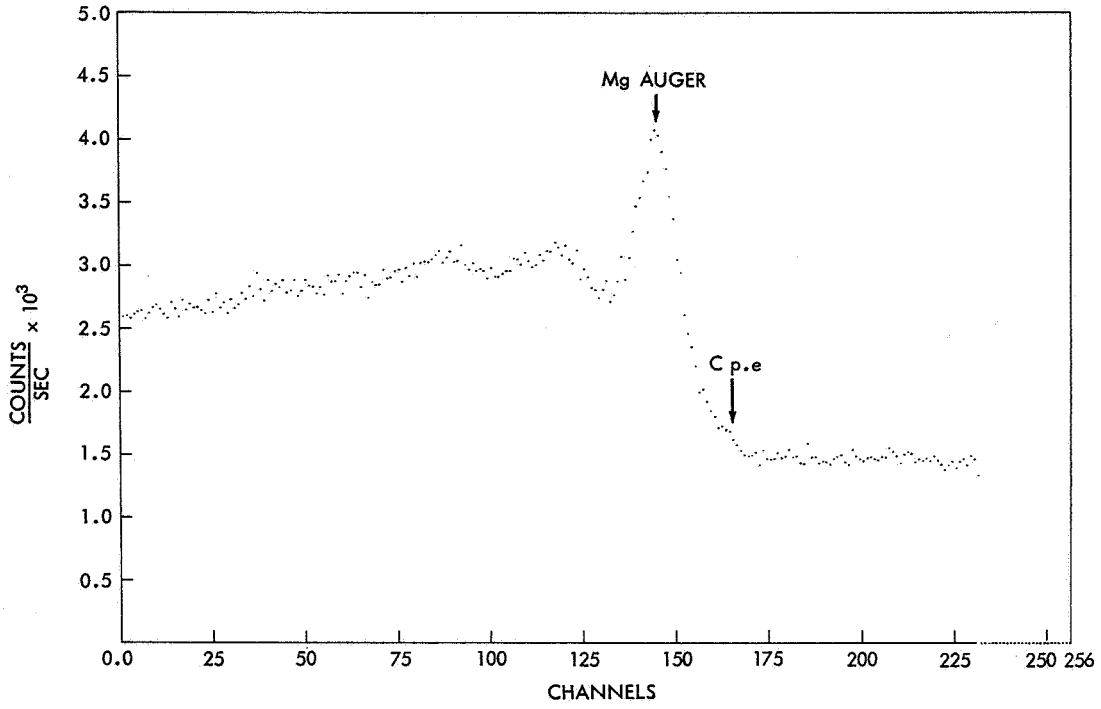

Figure 16. Fine scan of microscope slide sample. 1050-1320 eV, Al Kα excitation.

peak due to secondary electrons ejected from the spectrometer by the sample electrons. This peak is present in all spectra independent of sample material. Figure 15 shows the details of region of the highest peak in Figure 13. The photoelectron peak of O at 954 eV and Na KLL Auger peak at 989 eV are seen to be well separated in this display. Figure 16 is the fine scan of the Mg Auger line at 1180 eV and the C photoelectron peak at 1202 eV.

Figures 17-20 show the Cr Kα excited spectra of two representative rock samples GSP-1 (granite) and DTS-1 (dunite) obtained from the U. S. Geological Survey. The powdered rock sample were mixed with H_2O and brushed on a 6-μ mylar with very thinly coated graphite. Although both Auger and photoelectrons were present in these spectra attention was focused on the photoelectrons of Si, Al and Mg for the following reasons. First, the photoelectrons in this particular case have higher energies than the Auger electrons so that their structures are more distinct than the Auger group. Secondly, although not as important in the present case, the photoelectrons are truly monoenergetic for each element while a group of Auger lines exist as discussed in the INTRODUCTION. For the coarse resolution encountered here one sees essentially the strongest Auger transition KL_2L_3.

Table 1 lists the chemical elements of interest in these rock samples and their respective electron energies. In addition, C is also listed due to its presence as a surface contaminant. Table 2 shows the composition of the two rock

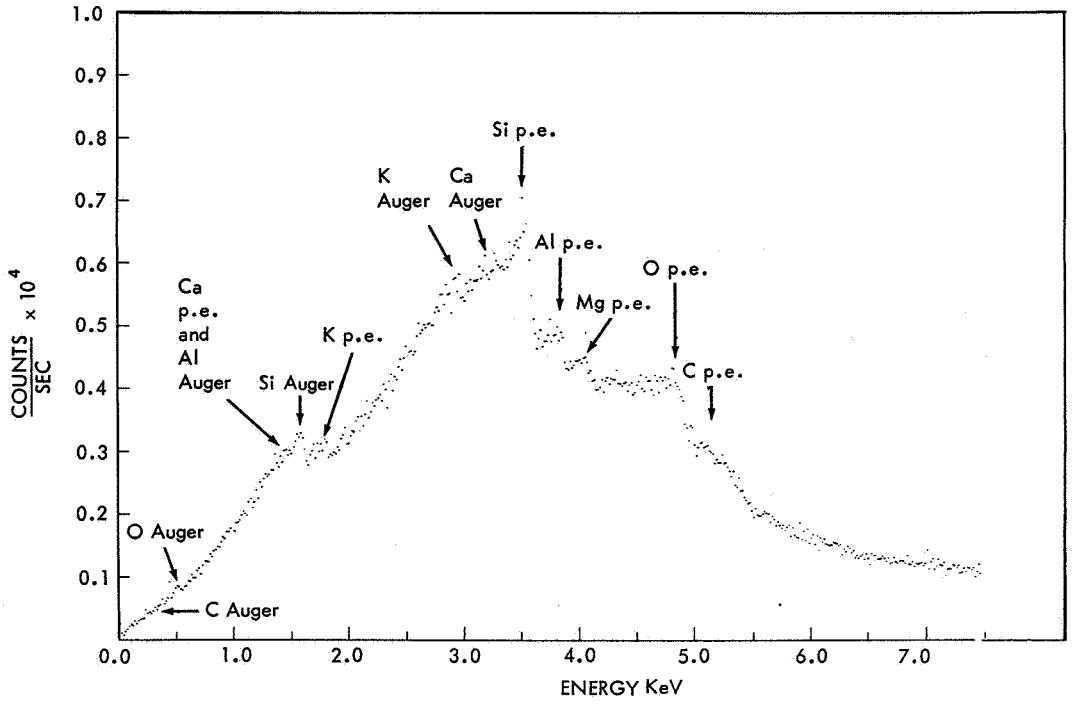

Figure 17. Coarse scan spectrum of GSP-1, 0-7500 eV, 16 eV/ch. Cr Kα excitation, x-ray anode at 15 kV, 80 ma.

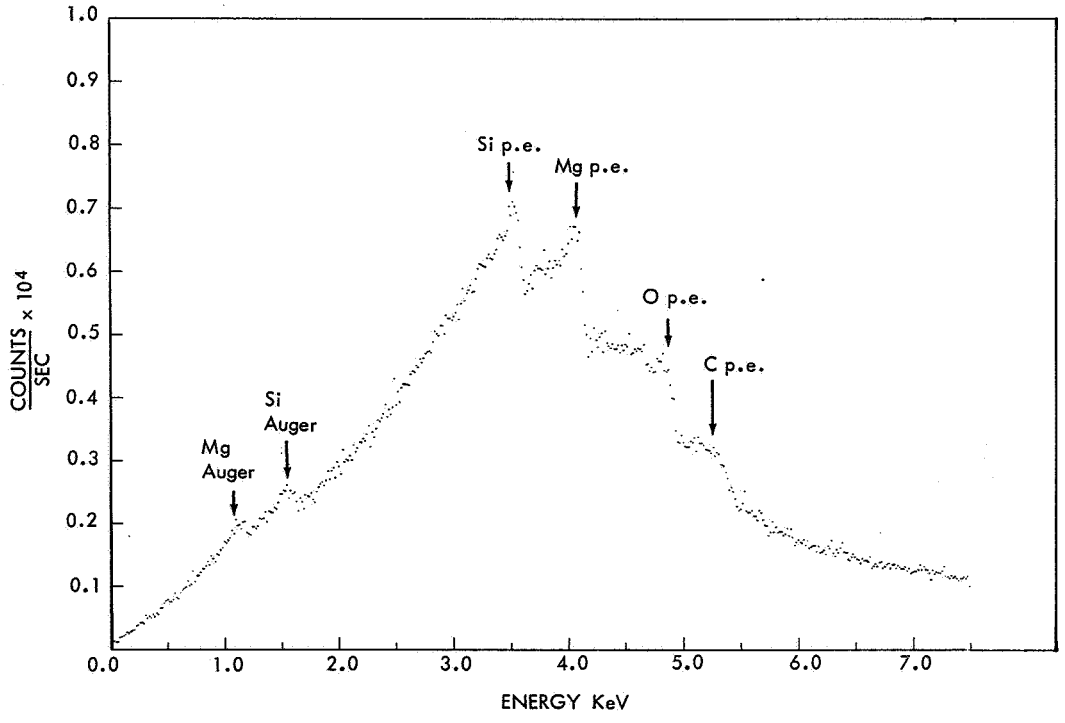

Figure 18. Coarse scan spectrum of DTS-1, 0-7500 eV, 16 eV/ch, Cr Kα excitation, x-ray anode at 15 kV, 80 ma.

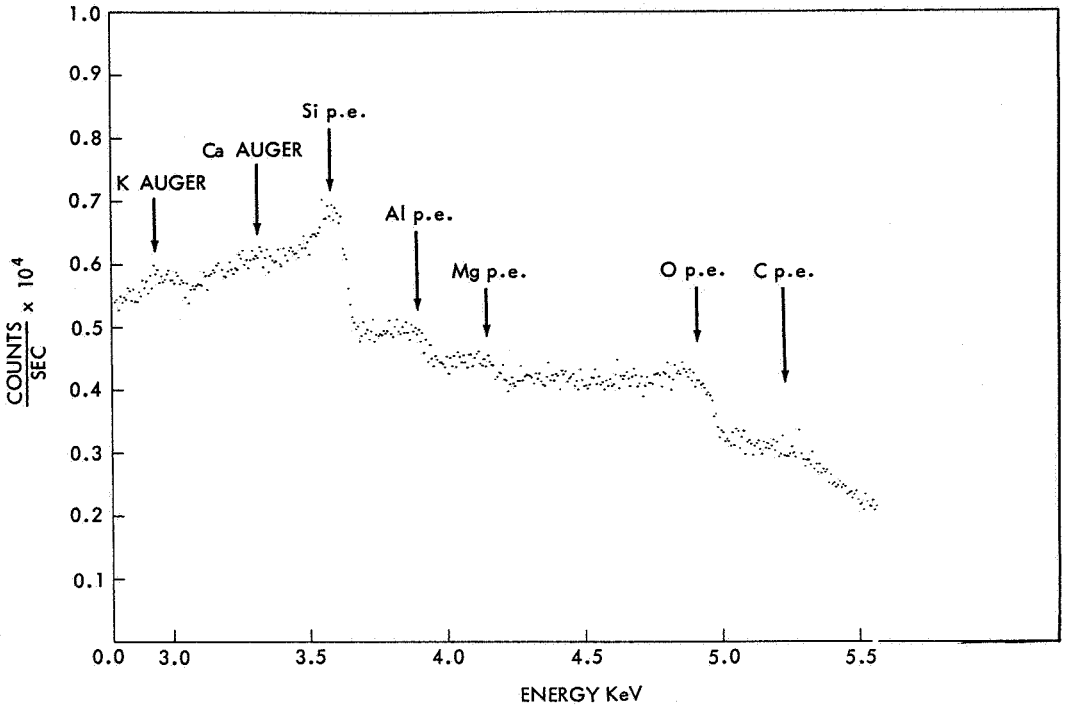

Figure 19. Medium scan spectrum of GSP-1, 2780-5560 eV, 6.7 eV/ch.
Cr Kα excitation, x-ray anode at 15 kV, 80 ma.

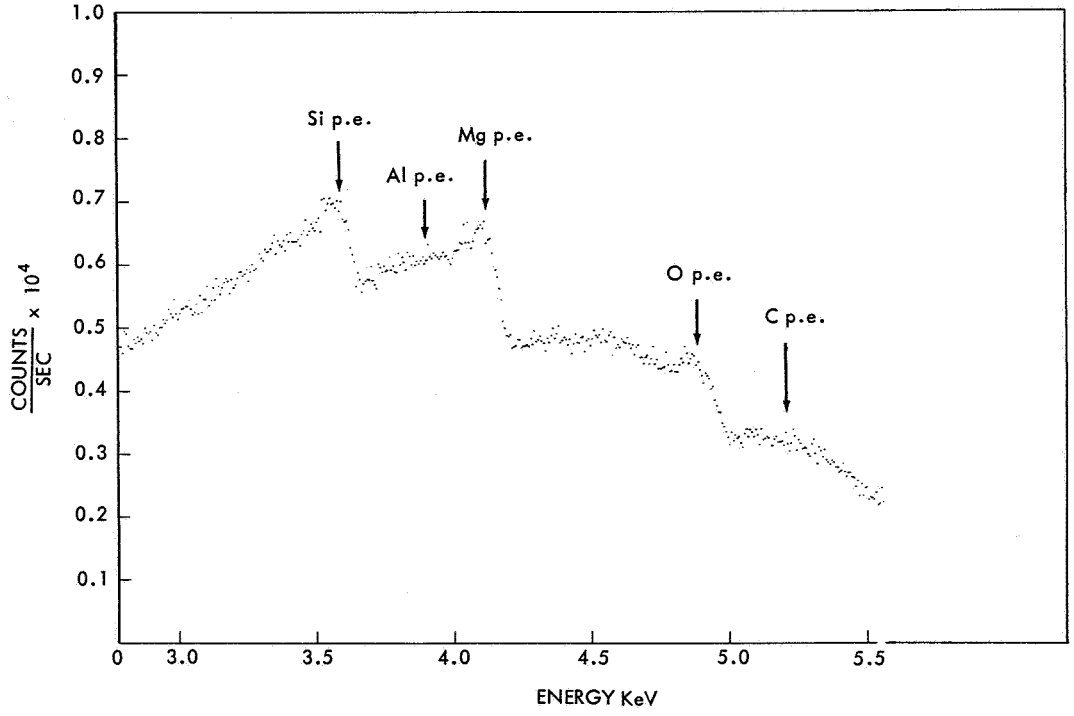

Figure 20. Medium scan spectrum of DTS-1, 2780-5560 eV, 6.7 eV/ch.
Cr Kα excitation, x-ray anode at 15 kV, 80 ma.

Table 1
Energies of Electrons Using Cr Kα Excitation

Element	Auger* KL_2L_3 (eV)	Photoelectron** (eV)
C	268	5131
O	516	4883
Mg	1180	4110
Al	1387	3855
Si	1607	3576
K	2965	1807
Ca	3286	1377

*Calculated from the approximate formula $E_{KL_2L_3}(Z) = E_K(Z) - E_{L_{II}}(Z) - E_{L_{III}}(Z+1)$
The binding energies are from Bearden and Burr, Revs. Mod. Phys. 39 125 (1967)

**Calculated from the binding energies in the reference cited above.

Table 2
Composition of GSP-1 and DTS-1
as Given by U. S. Geological Survey

Element	GSP-1	DTS-1
MgO	0.95%	49.83%
Al_2O_3	14.92%	0.30%
SiO_2	67.32%	40.48%
K_2O	5.52%	
CaO	2.06%	0.03%

samples as given by the U. S. Geological Survey. Figures 17 and 18 are the coarse scan spectra (0-7500 eV) of GSP-1 and DTS-1 respectively. The expected positions of various electron lines are indicated by arrows. Without detailed analysis it is interesting to observe the different coarse features caused by the different chemical compositions. In the Mg and Si Auger electron region, even with the poor statistics, DTS-1 (Figure 18) shows two distinct peaks while GSP-1 shows rather smeared bumps due to the contribution of Ca and K photoelectrons in the same region. Similarly on the low energy side of the Si photoelectron peak DTS-1 (Figure 18) shows a fairly constant slope while GSP-1 have bumps from the Auger electrons of K and Ca. The most pronounced feature is of course the difference in the Mg photoelectron peak between the two samples. Figures 19 and 20 are the medium scans of GSP-1 and DTS-1 respectively in the prominent photoelectron peaks region of 2780-5560 eV. Again one notes the presence of K and Ca Auger electrons in GSP-1 (Figure 19) as well as the big difference in Mg photoelectron peaks. As mentioned earlier, these are only qualitative observations, as yet no quantitative measurement of intensities have been attempted.

CONCLUSION

This preliminary study helped to establish some of the characteristic features, problems and capabilities of applied Auger and photoelectron spectroscopy. In order to obtain quantitative information or more accurate qualitative information a high vacuum system in the 10^{-9} or 10^{-10} torr range with cleaning facilities such as heating and glow discharging is necessary. Such a system is being designed at present. To measure intensities, the determination of the overall collection efficiency of the spectrometer-detector system as a function of energy must be made. When these have been accomplished one may then hope to realize some or all of the potential applications of Auger and photoelectron spectroscopy mentioned in the INTRODUCTION.

REFERENCES

1. P. Auger, Comptes Rendus 180 65 (1925).

2. G. Wenzel, Zeit. Phys. 43 524 (1927).

3. E. H. S. Burhop, J. Phys. Rad. 16 625 (1955).

4. H. L. Hagedoorn & A. H. Wapstra, Nuc. Phys. 15 146 (1960).

5. K. Siegbahn, Physica 8 1043 (1952).

6. K. Siegbahn & K. Edvarson, Nuc. Phys. 1 137 (1956).

7. K. Siegbahn ed. "Alpha-, Beta- and Gamma-Ray Spectroscopy" North-Holland Publishing Co. Appendix 2 (1965).

8. W. N. Asaad and E. H. S. Burhop, Proc. Phys. Soc. 71 369 (1958).

9. Ewan, Graham & Grodzins, Can. J. Phys. 38 163 (1960).

10. Graham, Bergstrom & Brown, Nuc. Phys. 39 107 (1962).

11. Hornfeldt, Fahlman & Nordling, Ark. Fys. 23 155 (1962).

12. O. Hornfeldt, Ark. Fys. 23 235 (1962).

13. W. N. Asaad, Nuc. Phys 44 399 (1963).

14. Erman, Bergstrom, Chu & Emery, Nuc. Phys. 62 401 (1965).

15. W. Mehlhorn & R. G. Albridge, Zeit. Phys. 175 506 (1963).

16. W. N. Asaad, Nuc. Phys. 66 494 (1965).

17. H. Korber & W. Mehlhorn, Zeit. Phys. 191 217 (1966).

18. Fahlman, Nordberg, Nordling & Siegbahn, Zeit. Phys. 192 476 (1966).

19. Y. Y. Lui & R. G. Albridge, Nuc. Phys. A92 139 (1967).

20. W. Mehlhorn and W. N. Asaad, Zeit. Phys. 191 231 (1966).

21. Johnston, Douglas & Albridge, Nuc. Phys. A91 505 (1967).

22. Hagstrom, Nordling & Siegbahn, Zeit. Phys. 178 439 (1964).

23. Axelson, Ericson, Fahlman, Hamrin, Hedman, Nordberg, Nordling & Siegbahn, Nature 213 No. 5071, 70 (1967).

24. Fadley, Hagstrom, Hollander, Klein & Shirley, UCRL-17426 (1967).

25. Fahlman, Hamrin, Nordberg, Nordling & Siegbahn, Phys. Letters 20 159 (1966).

26. Nordling, Hagstrom & Siegbahn, Zeit. Phys. 178 433 (1964).

27. L. A. Harris, Industrial Research 10 No. 2, 52 (1968).

28. W. Mehlhorn, Zeit. Phys. 160 247 (1960).

29. W. Mehlhorn, Zeit, Phys. 187 21 (1965).

30. E. M. Purcell, Phys. Rev. 54 818 (1938).

31. N. Ashby, Nuc. Instr. 3 90 (1958).

32. Ritchie, Cheka & Birkhoff, Nuc. Instr. & Methods, 6 157 (1960).

33. Birkhoff, Kohn, Eldridge & Ritchie, Nuc. Instr. & Methods 8 313 (1960).

34. Hubbell, McConnell & Birkhoff, Nuc. Instr. & Methods 31 18 (1964).

35. F. T. Rogers, Jr., Rev. Sci. Instr. 22 723 (1951).

36. Craig et al., Phys. Rev. 81 304 (1951), and Phys. Rev. 83 203 (1951).

37. Bader, Fryer & Witteborn, NASA TN D-1035 (1961).

38. Wolfe, Silva & Myers, J. Geophys. Res. 71 1319 (1966).

39. F. R. Paolini and G. C. Theodoridis, Rev. Sci. Instr. 38 579 (1967).

40. B. L. Henke, AFOSR - 1995 (1962), and Appendix II - Geometrical Optics.

41. H. Golstein, Classical Mechanics (Addison-Wesley Publishing Co., Inc., 1957) pp. 76-80.

42. K. C. Schmidt & C. F. Hendee, IEEE Trans. Nuc. Sci. NS-13 100 (1966).

43. R. D. Deslattes & B. G. Simson, Rev. Sci. Instr. 37 753 (1966).

44. K. W. Yee & R. D. Deslattes, Rev. Sci. Instr. 38 637 (1967).

45. L. A. Harris, J. Appl. Phys. 39 1419 (1968).

46. L. A. Harris, J. Appl. Phys. 39 1428 (1968).